

^b Institut de recherches sur la catalyse et l'environnement de Lyon (IRCELYON, UMR 5256, CNRS; Université Claude Bernard Lyon 1), 2 Avenue Albert Einstein, 69626 Villeurbanne Cedex, France

Received 5 May 2012
Received in revised form 16 June 2012
Accepted 20 June 2012
Available online 6 July 2012

- Ethanol steam reforming
- Catalyst deactivation
- Ir particle sintering
- Ceria restructuring
- Carbon deposition

The ageing processes of a model Ir/CeO₂ catalyst during ethanol steam reforming was investigated. Various causes of deactivation were identified, depending on reaction temperature and time on stream. The initial, fast and but rather limited deactivation process was ascribed essentially to a loss of ceria surface (smoothing by loss of microporosity and/or roughness in the presence of steam), coinciding with an active phase build-up formed by a monolayer of carbonaceous reacting intermediates. In addition, a progressive and long-term deactivation was found to superimpose, originating from structural changes at the ceria/Ir interface linked to the Ir particles sintering and the ceria restructuring. The continuous build-up of an encapsulating layer of carbon at moderate temperature, coming from C₂ intermediate polymerization, was found not to contribute significantly to the catalyst deactivation, at least under the operating conditions investigated in this study.

© 2012 Elsevier B.V. All rights reserved.

Steam reforming (SR) of bio-ethanol is seen as a sustainable route to feed on-line proton exchange membrane fuel cells (PEMFC) with hydrogen, using integrated systems [1]. As compared to partial oxidation (POX) and oxidative steam reforming (OSR), the ethanol SR is characterized by higher hydrogen yields, lower reaction rates and a marked endothermicity [2–7]. To date, Ni [8,9], Co [10], Rh [11–13] and Ir [14–16] catalysts have been extensively investigated for ethanol SR. Among them, CeO₂-supported Rh [12,13] and Ir [14,15] catalysts are ranked among the most efficient systems with respect to hydrogen yield and reaction rate. This was discussed in terms of a bifunctional mechanism combining the primary ethanol and water activation on the ceria support and the C–C bond breaking of the C₂ intermediates at the noble metal/ceria interface, stabilized by strong metal–support interactions. However, these catalysts also tend to deactivate with time on stream, because of the carbonaceous species deposition and/or the active phase sintering [17,18]. The detailed role and relative importance of these ageing phenomena have not been clearly analyzed till now.

change the selectivity [19–21]. From the sequential steps involved in the reforming process, the primary activation of ethanol on the catalytic support may lead to a first group of C_{2+} products, such as ethylene, acetaldehyde and/or acetone via dehydration, partial oxidation and condensation/decarbonylation reactions, respectively, depending on the type of acidic and/or basic sites on the oxide support [14]. These products may eventually be converted to carbonaceous deposits depending on contact time and temperature [19,22]. For example, the formation of ethylene was shown to provoke a severe carbon deposition on a Co/Al_2O_3 catalyst in the ethanol SR [23]. Similarly, the acetaldehyde formed preferentially on a Co/ZnO catalyst was also found to further polymerize to carbonaceous species, leading to the active sites blockage [24]. On the contrary, these C_{2+} primary products can undergo further cracking into C_1 intermediates to produce syngas, as targeted in the SR process. At that point, other types of carbon deposition may occur on the metal phase, such as filamentous or encapsulating graphite formed from various C_1 condensation and/or carbide formation processes. The nature and dispersion of the metal (noble or non noble) were found to strongly influence these processes [8]. Thus, two types of carbon deposits were observed on an aged ethanol SR Ni/Al_2O_3 catalyst, being located on both the active metal and the support surface [8]. Similarly, deposition of graphite or polyaromatics resulted in severe deactivation of Rh/Al_2O_3 and $Rh/Ce_{0.8}Zr_{0.2}O_2-Al_2O_3$ catalysts [25].

If one considers now the catalyst sintering as another potential ageing process, both metal particles and support grains sintering were observed under reforming conditions. Thus, in our previous

work on Ir/ceria catalysts in the steam reforming or the oxidative steam reforming [14,15], it was observed that under the severe conditions of ethanol reforming, the initially well-dispersed metal and ceria particles tended to sinter at different levels, resulting (i) in an increase of the crystallinity and a decrease of the structural defect concentration of the ceria support, and (ii) in a loss of metal dispersion, involving a major decrease in the metal–support interactions after long-term runs.

In this work, we investigated to a deeper extent the deactivation of a model Ir/CeO₂ catalyst under ethanol SR conditions in order to unravel the specific effect of each of the above mentioned ageing causes. This catalyst was selected among a large series of materials since it presents a high initial dispersion of both Ir and ceria, therefore offering a high catalytic activity in the ethanol SR and then leading to large coke deposition rates and significant morphological changes. The deactivation rates observed at various reaction temperatures and contact times are analyzed on the basis of the observed changes in texture/structure of the catalyst and in the amount and type of carbonaceous deposits accumulating during long-term runs.

2. Experimental

2.1. Catalyst preparation

The CeO₂ support was prepared by precipitation of cerium(III) nitrate with urea in aqueous solution, while the Ir/CeO₂ catalyst with an Ir nominal loading of 2.0 wt.% was prepared by a deposition-precipitation method as described elsewhere [14]. After filtration and washing with hot water and ethanol, the resulting solid was dried at 373 K overnight and calcined at 923 K for 5 h in static air.

2.2. Catalyst testing

Ethanol SR was conducted in a continuous-flow fixed-bed tubular quartz reactor. 25 mg of the as-prepared catalyst (40–60 mesh) was loaded and sandwiched between two layers of quartz wool. The catalyst was then reduced under 10% H₂/He mixture (50 mL min^{−1}) at 673 K for 1 h. The flow was then turned to pure He (30 mL min^{−1}) and the temperature was set at 673–923 K. An aqueous ethanol/water solution was injected (1:3 stoichiometric molar ratio), using a micro-pump, into a vaporizer heated to 473 K and then introduced undiluted into the reactor at a gas hourly space velocity (GHSV) of 72,000 or 360,000 mL g^{−1} h^{−1}, corresponding to ethanol flow rates of 7.5 and 37.5 mL min^{−1} over 25 mg of catalyst, respectively. For each catalytic test corresponding to given time on stream, a new sample of the as-prepared catalyst was reduced in situ according to the above protocol. The effluent from the reactor was analyzed by on-line gas chromatography. H₂, CO, and CO₂ were separated using a packed column (HaySep D) and analyzed using a thermal conductivity detector (TCD). Hydrocarbons and oxygenates were separated using a capillary column (INNOWAX) and analyzed using a flame ionization detector (FID). The conversion of ethanol was determined from the concentration in the inlet and outlet streams, and the molar distribution of the outlet flow was calculated on the basis of the dry gas composition, that is by excluding water [14]. The latter will be named “outlet dry gas composition” in the following. The overall mass balance was always kept within ±3%.

2.3. Catalyst characterization

The actual Ir loading was analyzed by inductively coupled plasma atomic emission spectrometry (ICP-AES), using a PLASMA-SPEC-II instrument. An appropriate amount of the sample was

dissolved in aqua regia, and the mixture was diluted with nitric acid to meet the detection range of the instrument.

Nitrogen adsorption–desorption isotherms were recorded using an ASAP2020 instrument (Micromeritics). Before the measurement, the sample was degassed at 573 K for 3 h. The surface area was calculated by a multipoint BET analysis of the nitrogen adsorption isotherm.

X-ray diffraction (XRD) patterns were recorded on a D/MAX-RB diffractometer (Rigaku) with a Ni-filtered Cu K α radiation source that was operated at 40 kV and 100 mA. The mean crystalline size of ceria was calculated from the Scherrer equation [26].

Transmission electron microscopy (TEM) images were taken on a FEI Tecai G² F30S-Twin microscope operated at 300 kV. Specimens were prepared by ultrasonically suspending the sample in ethanol. Droplets of the suspension were deposited on a thin carbon film supported on a standard copper grid and dried in air.

Temperature-programmed reduction (TPR) of the as-prepared catalyst was performed with an Auto Chem II 2920 chemisorption analyzer using a thermal conductivity detector (TCD). 100 mg samples were loaded and pretreated under flowing Ar (50 mL min^{−1}) at 573 K for 1 h. After cooling down to 233 K, a 10% H₂/Ar (50 mL min^{−1}) mixture was introduced on the sample and the temperature was increased to 1073 K at a rate of 10 K min^{−1}.

Hydrogen chemisorption was performed with an Auto Chem II 2920 chemisorption analyzer at 233 K to inhibit the hydrogen spillover [27]. Since the loading of 20 mg for testing experiments was not large enough to make relevant chemisorption measurements, parallel ageing experiments using 100 mg catalyst were carried out for that purpose, keeping the GHSV constant (but without GC analysis).

The samples were oxidized with a 20% O₂/N₂ mixture at 873 K, followed by reduction with a 10% H₂/Ar mixture (50 mL min^{−1}) at 673 K for 1 h. After being cooled down to 233 K under flowing Ar (50 mL min^{−1}), pulses of hydrogen were injected until saturation and the total hydrogen uptake was determined. The sample was then flushed with Ar for 10 min to remove the physically adsorbed hydrogen and hydrogen pulses were then injected again until saturation. The mean Ir particle size was calculated according to the amount of chemically adsorbed hydrogen and considering the stoichiometry H/Ir_s = 1.

Temperature-programmed oxidation (TPO) of the used catalysts after various time on stream was conducted in a fixed-bed micro-reactor connected to a mass spectrometer (Omistar, Blazer). The used sample was initially heated to 573 K under flowing Ar to eliminate contaminants and possibly few unstable adspecies like weakly bonded carbonates or hydroxyl groups. It was checked that only minor amounts of CO₂ were desorbed during that initial cleaning step. After being cooled down to room temperature, the sample was heated to 1073 K at a rate of 5 K min^{−1} under a flow of a 5% O₂/Ar mixture (50 mL min^{−1}). The effluent composition (CO₂) was monitored by mass spectrometry.

3. Results and discussion

3.1. Unreacted catalyst characterization

ICP analysis showed that the actual Ir loading was 1.88 wt.% in the as-prepared catalyst with a surface area of 77 m² g^{−1}.

Fig. 1 shows the H₂-TPR profile of the as-prepared catalyst, displaying three distinct reduction peaks. In line with our previous studies [14,15], the reduction peak at about 463 K (ca. 355 $\mu\text{mol g}_{\text{cat}}^{-1}$) is assigned to both the reduction of IrO₂ species to metallic Ir (corresponding to an hydrogen consumption ca. 200 $\mu\text{mol g}_{\text{cat}}^{-1}$) and the partial reduction of the ceria surface (from Ce⁴⁺ to Ce³⁺), most likely around the Ir particles, where

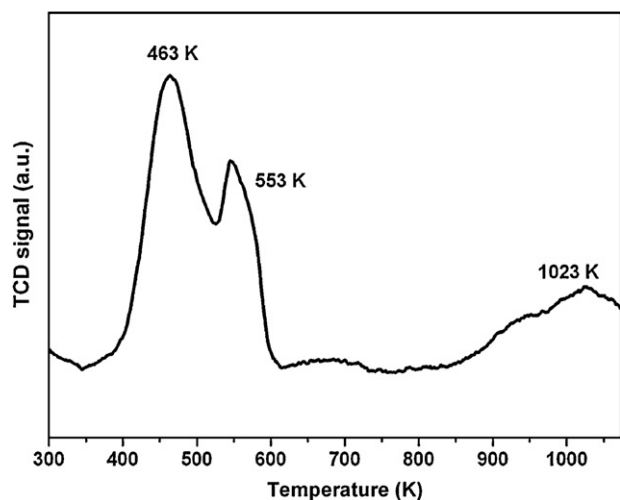


Fig. 1. H_2 -TPR profile of the as-prepared catalyst.

hydrogen can easily spill over from the reduced Ir particles to the ceria surface [28]. Note that the reduction of one monolayer of ceria would necessitate around $1600 \mu\text{mol g}_{\text{cat}}^{-1}$ of hydrogen, considering the initial BET surface and a mean surface oxygen density of ca. $21 \mu\text{mol m}^{-2}$. From this value, it can be inferred that the peak at 553 K (ca. $251 \mu\text{mol g}_{\text{cat}}^{-1}$) would correspond to the reduction of a part of the ceria surface located far from the Ir particles (where the spillover effect is less marked) and the broad peak at much higher temperature (maximum at 1023 K, around $139 \mu\text{mol g}_{\text{cat}}^{-1}$) would correspond to a partial reduction of the ceria bulk. By integrating the whole amount of hydrogen consumed (about $745 \mu\text{mol g}_{\text{cat}}^{-1}$) and accounting for the amount of hydrogen necessary for the Ir oxide reduction ($200 \mu\text{mol g}^{-1}$), the final stoichiometry of the reduced ceria sample was estimated to be ca. $\text{CeO}_{1.91}$. This corresponds quite well to the quantitative evaluation of the ceria reducibility deduced from OSC measurements, as reported on similar samples in [15]. It was shown that only one to two monolayers of the oxide were reduced, i.e. less than 20% of the maximum possible reduction of CeO_2 to Ce_2O_3 .

Fig. 2 shows the XRD patterns of the as-prepared and the reduced samples. The diffraction lines of ceria with fluorite structure were clearly observed in both cases. The mean crystallite sizes of ceria were about 8 nm in both cases. However, the diffraction

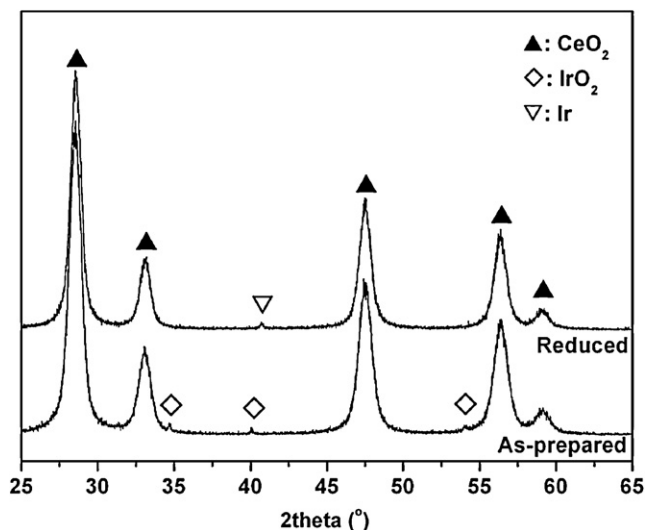


Fig. 2. XRD patterns of the as-prepared and the reduced catalysts.

line intensities in the reduced sample weakened considerably and the diffraction positions shifted towards lower 2θ values because of the defects that were generated by the reduction of the surface of ceria [14]. In addition, minor diffraction lines characteristic of IrO_2 and Ir species were also detected in the as-prepared and the reduced samples, respectively.

Fig. 3 shows the TEM images of the as-prepared and the reduced catalysts. For the as-prepared sample (Fig. 3A and B), the size of the spherical ceria particle was in the range of 5–10 nm, in good agreement with the XRD measurements, which tends to indicate that the ceria particles were almost single crystals. The IrO_2 particles, with a size of about 5–7 nm, were found to be well-dispersed and in tight contact with the ceria grains. After hydrogen reduction (Fig. 3C and D), the Ir particles (ca. 6 nm in size) were still homogeneously distributed and in tight contact with the ceria grains (ca. 5–10 nm, with well-defined edges). From these results, it was calculated (assuming cubic Ir particles) that the metallic surface in the reduced catalyst only accounts for 1.2% of the total BET surface developed by the sample, the rest being essentially Ce_2O_3 or CeO_2 , depending on the redox conditions. This percentage, which may change slightly upon catalyst sintering, will be used further on to discuss the bifunctional mechanism of the ethanol SR.

3.2. Ageing analysis under ethanol SR conditions

In order to study the ageing phenomena on the Ir/CeO₂ catalyst occurring under steam reforming conditions, we first checked the influence of the reaction temperature on the catalytic performances, by raising the temperature with the same catalyst sample, waiting at each temperature a stabilized conversion.

Then, long-term stability (40–60 h on stream) was tested over the temperature range 773–923 K, i.e. under conditions where the reaction mechanism changes deeply from mainly ethanol dehydrogenation to mainly reforming into syngas (including WGS/RWGS equilibrium). Here, for each ageing experiment, a fresh catalyst was reduced in situ and contacted with the same ethanol/steam feedstock. A series of analyses (BET, XRD, and TPO) were performed at key steps of the ageing processes, as it will be presented later.

3.2.1. Influence of the reaction temperature on catalytic performances

Fig. 4 illustrates the temperature-dependence of the ethanol conversion and the outlet dry gas composition in the ethanol SR over the Ir/CeO₂ catalyst. The conversion of ethanol increased progressively with increasing temperature. However, since these changes in catalytic performances with temperature also included temperature sensitive ageing phenomena (changes in texture and structure and/or carbon deposition) as it will be discussed later, no calculation of the apparent activation energy was attempted. Concerning the outlet dry gas composition at 673 K, the main constituent was indeed the unconverted ethanol (ca. 90%) while mainly acetaldehyde was produced (ca. 6% together with around 4% of hydrogen), indicating that only the primary dehydrogenation of ethanol occurred at low temperature. At 773 K, in addition to the still large production of acetaldehyde, the production of CO_2 , CO and H_2 (now the main product) was also observed, in agreement with the expected thermodynamic equilibrium calculated for the ethanol steam reforming ($\text{H}_2:\text{CO}_2:\text{CO} = 19:9:2$), as represented in Fig. 5. Noteworthy, this product distribution is essentially governed by the WGS/RWGS equilibrium. Furthermore, the quasi absence of methane is related to the weak methanation activity of Ir. By further increasing the temperature to 873 K, the concentration of CO, CO_2 and CH_4 in the outlet dry gas composition still increased, always close to the thermodynamic equilibrium, while the concentration of acetaldehyde decreased markedly. This demonstrates that the primary route towards acetaldehyde formation is replaced

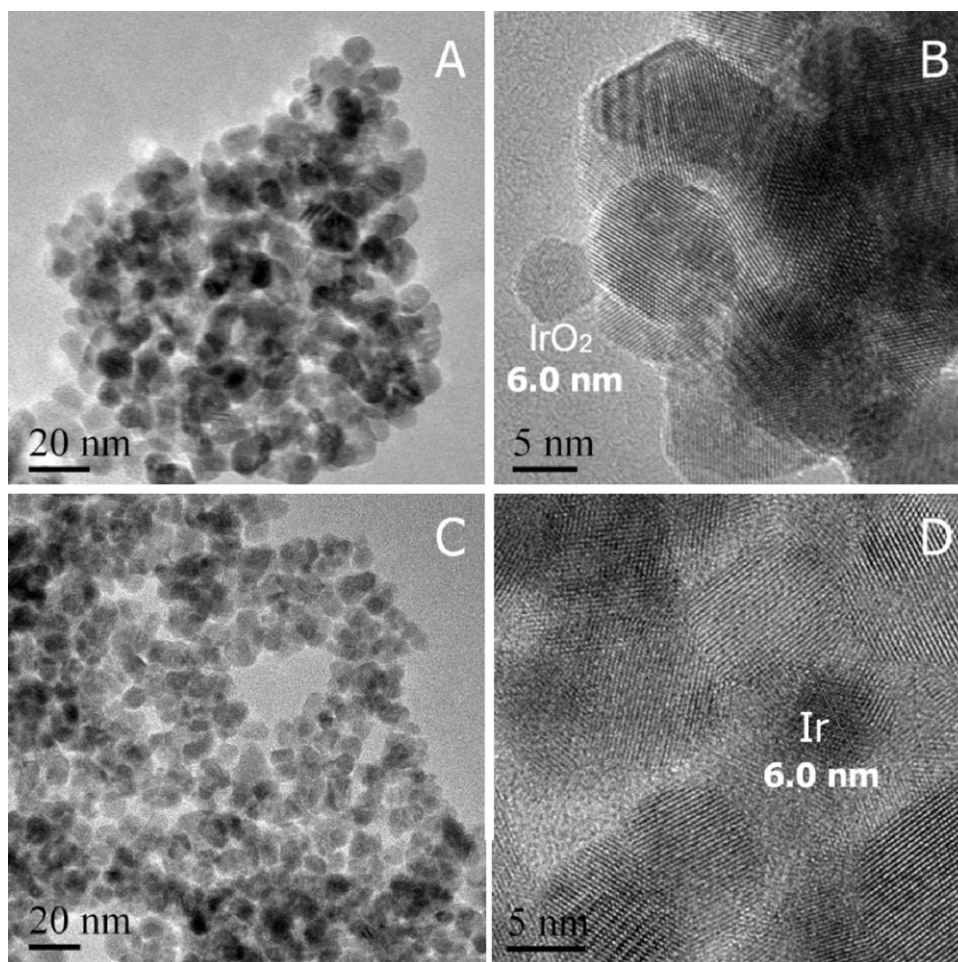


Fig. 3. HRTEM images of the as-prepared (A–B) and the reduced (C–D) catalysts.

progressively by the secondary steam reforming of ethanol into syngas and methane, as expected from thermodynamics. At 923 K, the conversion of ethanol approached 78% and the outlet dry gas composition consisted of 51% H₂, 19% CO, 17% CO₂, 4% CH₄ (including 9% of unconverted ethanol), again matching quite closely with

the thermodynamic equilibrium calculated for the ethanol SR conditions (Fig. 5). Therefore, in perfect agreement with the trends already observed either in the SR or the oxidative SR of ethanol [14,15,29], one can see that the progressive changes in selectivity with temperature reflect the changes in the mechanistic routes. At low temperature, the primary dehydrogenation of ethanol into

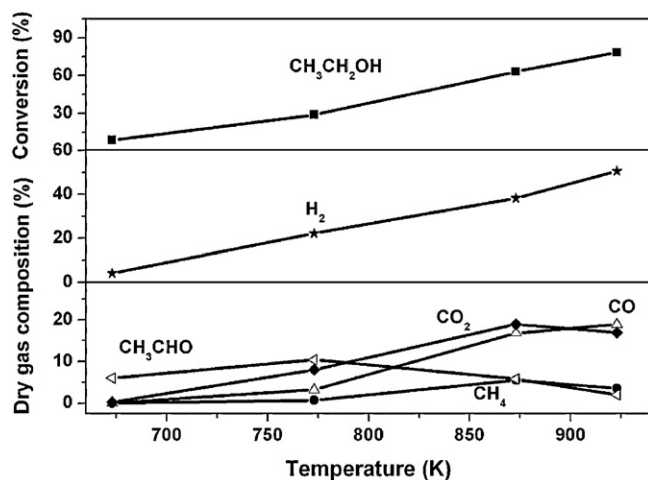


Fig. 4. Ethanol conversion and outlet dry gas composition during ethanol steam reforming over the Ir/CeO₂ catalyst (the balance in the outlet dry gas composition corresponds to the unconverted ethanol). Reaction conditions: mass of catalyst: 25 mg, C₂H₅OH/H₂O = 1:3 (molar ratio), GHSV = 72,000 mL g⁻¹ h⁻¹.

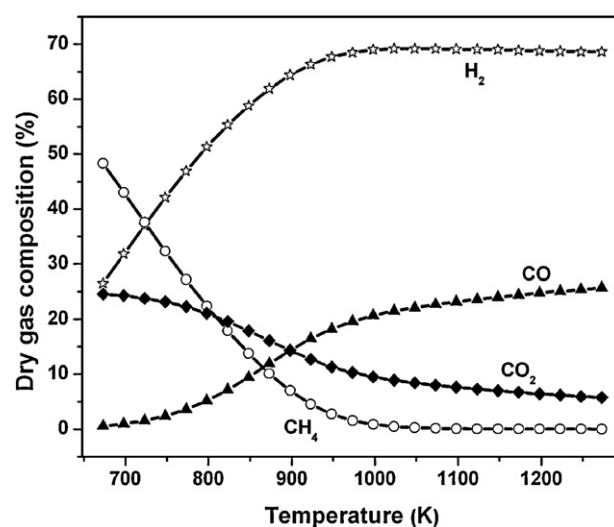


Fig. 5. Thermodynamic equilibrium of dry gas composition for the ethanol SR as a function of temperature (EtOH/H₂O = 1/3, pressure: 1 atm).

acetaldehyde involves essentially the ceria surface as the active phase (via ethoxy and acetate intermediates), as demonstrated in [14,15]. At medium temperature, this route is progressively replaced by the syngas chemistry involving the migration and decomposition of these C_2 adspecies at the Ir/ceria interface where they are cracked into C_1 adspecies (carbonyls, methyls and carbonates) to form the equilibrated $CO/CO_2/H_2$ mixture. At higher temperature, the metallic catalysis dominates and the methane, formed from the cracking of the acetates, can be converted by steam reforming into syngas. The question now arises how these changes in surface chemistry and catalytic performances are sensitive to the ageing phenomena occurring under these reaction conditions.

3.2.2. Activity decay at various conditions

A first ageing experiment was carried out at rather low temperature (773 K) and low space velocity ($GHSV = 72,000 \text{ mL g}^{-1} \text{ h}^{-1}$) to focus on the initial deactivation. The same experiment carried out at higher temperature led to a complete initial conversion of ethanol, obscuring any ageing information. As can be seen in Fig. 6, the conversion of ethanol was about 30% after 40 min on stream but it decreased to 10% after 5 h on stream, to practically level off at longer time on stream (TOS) (ca. 8% after 60 h on stream). During this fast initial deactivation process, the concentration of hydrogen in the dry gas outlet decreased from 30% to 16%, while the one of acetaldehyde slightly decreased from 9% to 5%. Traces of ethylene were detected. The concentrations of CO_2 , CO and CH_4 were only slightly fluctuating during this initial period, keeping the overall carbon balance equilibrated. These latter concentrations were then levelling up over the whole test.

A second series of experiments was carried out at higher space velocity ($GHSV = 360,000 \text{ mL g}^{-1} \text{ h}^{-1}$) over the whole range of temperature (773–923 K), with only a partial conversion over the testing period at any temperature. To avoid the unstable initial period already studied (Fig. 6), the first activity measurements were taken after 2 h on stream, allowing to concentrate on the slow ageing processes only.

As can be seen on Fig. 7A, the conversion of ethanol decreases to a larger extent at higher reaction temperatures. In order to check if a similar ageing process was governing this decay in activity, we normalized all the curves by dividing each data point by the initial conversion value, as depicted in Fig. 7B. Even though all curves tend to follow similar trends (within experimental uncertainty), it seems that the deactivation rate is slower at 773 K than at the other

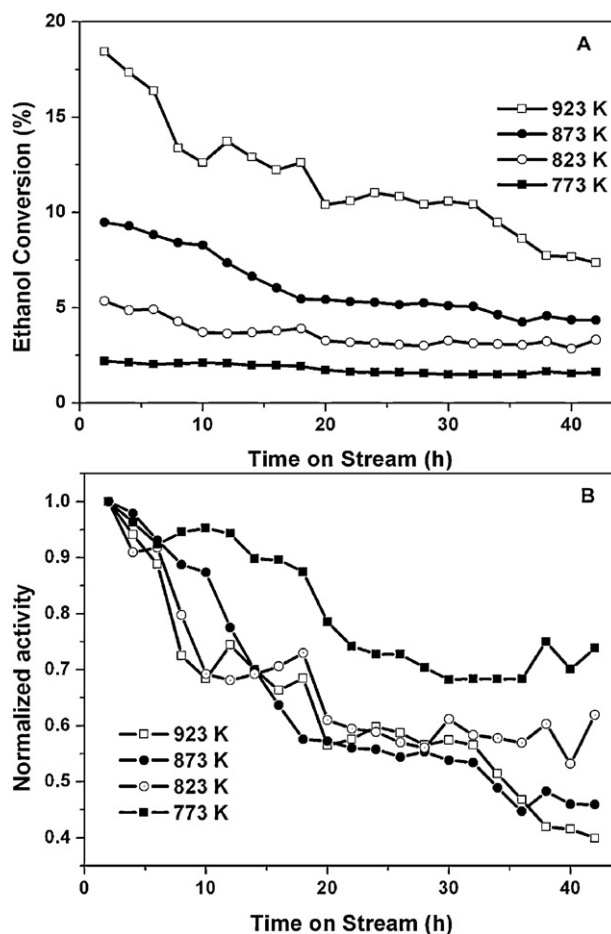


Fig. 7. Ethanol steam reforming over the Ir/CeO₂ catalyst at 773–923 K. Reaction conditions: mass of catalyst: 5 mg, $C_2H_5OH/H_2O = 1:3$ (molar ratio), $GHSV = 360,000 \text{ mL g}^{-1} \text{ h}^{-1}$. A: Raw data, B: normalized data.

temperatures, as it will be discussed later on. We will analyze in more detail the decay curves corresponding to the two extreme temperatures, i.e. 773 and 923 K, on the basis of the catalyst changes in terms of morphology and structure during these long-term tests.

3.2.3. Changes in catalyst structure/texture/morphology with time on stream

Fig. 8 shows the XRD patterns of the used Ir/CeO₂ catalyst sampled at different time intervals during the ageing test at 773 K. Typical diffraction lines of CeO₂ are detected for all samples, and the mean crystallite size keeps constant ca. 8 nm, similarly to what was measured on the as-prepared sample. This result indicates that the crystalline structure of the ceria grains remained rather stable at such relatively low temperature, as expected from its pretreatment under air at 923 K. Table 1 compares the BET values of the fresh catalyst (as prepared and reduced) and after different TOS (2 and 60 h). A significant loss of surface area was observed after the first 2 h on stream with a decrease from 77 to $61 \text{ m}^2 \text{ g}^{-1}$, while a moderate loss of surface was observed after 60 h on stream ($56 \text{ m}^2 \text{ g}^{-1}$). Close results were reported and analyzed by Pijolat et al. [31] showing that a fast loss of BET surface occurred as soon as a calcined ceria was contacted by steam at 943 K, followed by a much slower sintering process. A surface restructuring leading to the loss of microporosity was proposed for the fast initial loss of surface. Other types of slower morphological restructuring under ethanol steam reforming conditions underline the crucial role of the $\{100\}/\{110\}$ -surface structures as compared to the more dense $\{111\}$ faces [30].

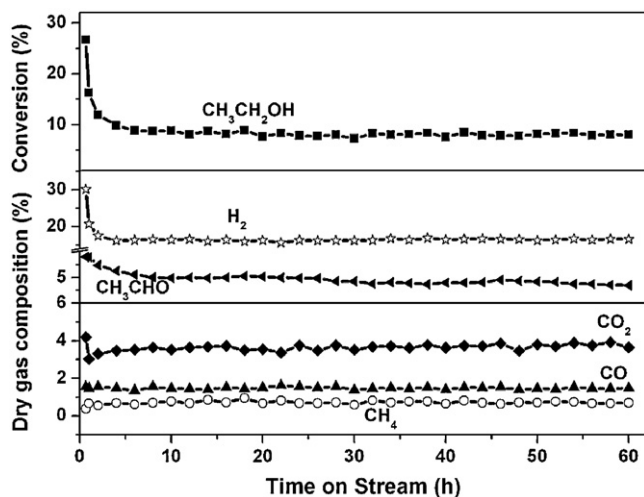


Fig. 6. Ethanol steam reforming over the Ir/CeO₂ catalyst at 773 K. Reaction conditions: mass of catalyst: 25 mg, $C_2H_5OH/H_2O = 1:3$ (molar ratio), $GHSV = 72,000 \text{ mL g}^{-1} \text{ h}^{-1}$.

Table 1
Changes in structure/morphology according to the reaction temperature and the time on reforming stream. Reaction conditions: mass of catalyst: 25 mg, $C_2H_5OH/H_2O = 1:3$ (molar ratio), GHSV = 360,000 mL g⁻¹ h⁻¹.

| 773 K | | | | | | | | | |
|---------------|---------------------------------------|--|------------------------------------|-------------------|---------------------|------------------------|--|-------------------------|--------------------------|
| | BET (m ² g ⁻¹) | Ceria size (d _{CeO₂} , nm) | Ir size (d _{Ir} , nm) | Ir dispersion (%) | EtOH conversion (%) | EtOH rate (μmol/(g s)) | Intrinsic rate (μmol/(m ² s)) | Deactivation degree (%) | Carbon deposits (mg C/g) |
| Initial (2 h) | 61 (77 ^d) | 8 ^b | 6 ^a (6.3 ^b) | 16.7 | 0.02 | 24.5 | 0.39 (1.9 ^e) | | 10 ^c |
| Final (60 h) | 56 | 8 ^b | 9.6 ^b | 10.4 | 0.01 | 10.2 | 0.18 (1.7 ^e) | 42.7 | 30 ^c |
| 923 K | | | | | | | | | |
| | BET (m ² g ⁻¹) | Ceria size (d _{CeO₂} , nm) | Ir size (d _{Ir} , nm) | Ir dispersion (%) | EtOH conversion (%) | EtOH rate (μmol/(g s)) | Intrinsic rate (μmol/(m ² s)) | Deactivation degree (%) | Carbon deposits (mg C/g) |
| Initial (2 h) | 57 (77 ^d) | 8 ^b | 6 ^a | 16.7 | 0.17 | 173.8 | 3.04 (18.2 ^e) | | 5.0 ^c |
| Final (60 h) | 47 | 9 ^b | 10.5 ^b | 9.5 | 0.08 | 77.7 | 1.65 (17.4 ^e) | 26.8 | 7.2 ^c |

^a Data obtained from the HRTEM images for the fresh catalyst.

^b Data obtained from the XRD patterns of the catalysts reacted.

^c Data obtained from the TPO patterns of the catalysts reacted.

^d Sample reduced but unreacted.

^e Intrinsic rate divided by Ir dispersion and multiplied by 100 dispersion = 1/d_{Ir}, deactivation degree = (initial rate – final rate)/initial rate.

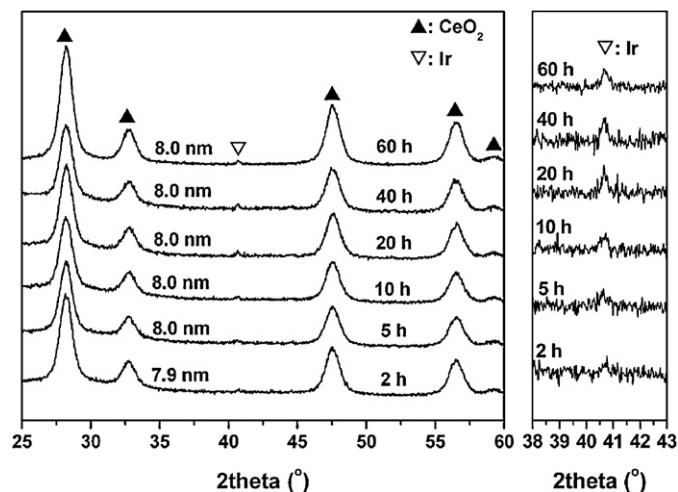


Fig. 8. XRD patterns of the used Ir/CeO₂ catalysts at different time on stream. Reaction conditions: mass of catalyst: 25 mg, $C_2H_5OH/H_2O = 1:3$ (molar ratio), GHSV = 72,000 mL g⁻¹ h⁻¹, $T_{\text{reaction}} = 773$ K. Six separate ageing experiments were performed for each XRD characterization. For each experiment, the same pretreatment and reaction conditions were applied, except that the time on stream was varied from 2 to 60 h.

Concerning the Ir particles, characteristic diffraction lines appeared after 2 h on stream and the intensity increased slightly with longer time on stream, indicative of a significant increase of the Ir mean particle size from 6 to 9 nm. Hydrogen chemisorption measurements confirmed that the average size of the Ir particles increased from 6 nm at the beginning (2 h on stream) to 9 nm after 60 h on stream. This rather limited sintering process, which corresponds to a decrease of the Ir dispersion from ca. 17 to 11%, was expected from the initial high temperature treatment (923 K), leading to a relatively low initial Ir dispersion, on the contrary to other well dispersed catalysts we reported in previous studies [14,15].

Fig. 9 shows HRTEM images of the Ir/CeO₂ samples aged at 773 K at different TOS. After 2 h on stream (Fig. 9A and B), the size of the Ir particles was ca. 6 nm, i.e. unchanged as compared to the fresh catalyst sample. After 5 h on stream (Fig. 9C and D), the Ir particles were still 6 nm on average, but a thin layer of amorphous carbon could clearly be seen on the catalyst surface and some particles (Ir and ceria) were fully covered by carbonaceous deposits. After 20 h on stream (Fig. 9E and F), the Ir particle size has increased to 9 nm and heavy carbon deposition occurred, covering the surface of both the Ir particles and the ceria support. After 60 h on stream (Fig. 9G and H), the carbon deposits almost fully covered the catalyst surface and the size of the Ir particles was maintained around 9 nm. It was also observed by TEM in Fig. 9 and on other pictures not reported here some changes in the ceria crystallite shape all along the ageing process, with a slow ceria restructuring from spherical crystallites (initial state) to polygonal cubes (after long period on stream).

A rationale of all these changes in catalyst structure/texture/morphology with time on stream at the relatively low temperature of 773 K can be formulated as follows:

- No major changes in the structure/texture of the ceria were noted by XRD and TEM after the initial 2 h on stream period. Therefore, the fast initial decrease in the BET surface is deemed to come from a smoothing effect (i.e. loss of surface roughness and/or microporosity) induced by the presence of steam [31] and the build-up of a carbonaceous layer, as will be described later.
- In turn, the slow and regular decrease of the BET surface (from 61 to 56 m² g⁻¹ after 60 h on stream) would correspond to ceria

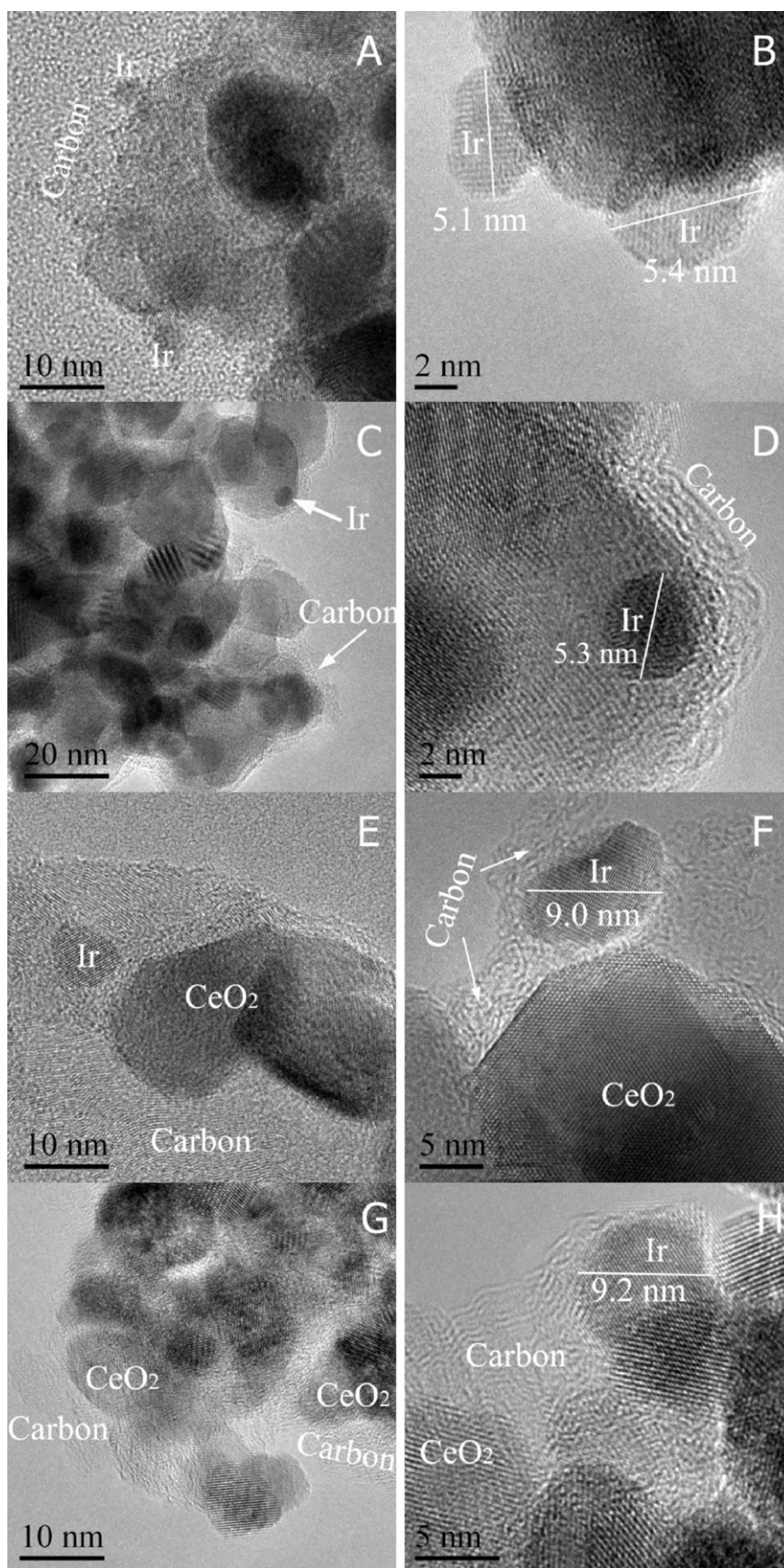


Fig. 9. HRTEM images of the used Ir/CeO₂ catalysts: A–B, 2 h; C–D, 5 h; E–F, 20 h; G–H, 60 h. Reaction conditions: mass of catalyst: 25 mg, C₂H₅OH/H₂O = 1:3 (molar ratio), GHSV = 72,000 mL g⁻¹ h⁻¹, $T_{\text{reaction}} = 773$ K.

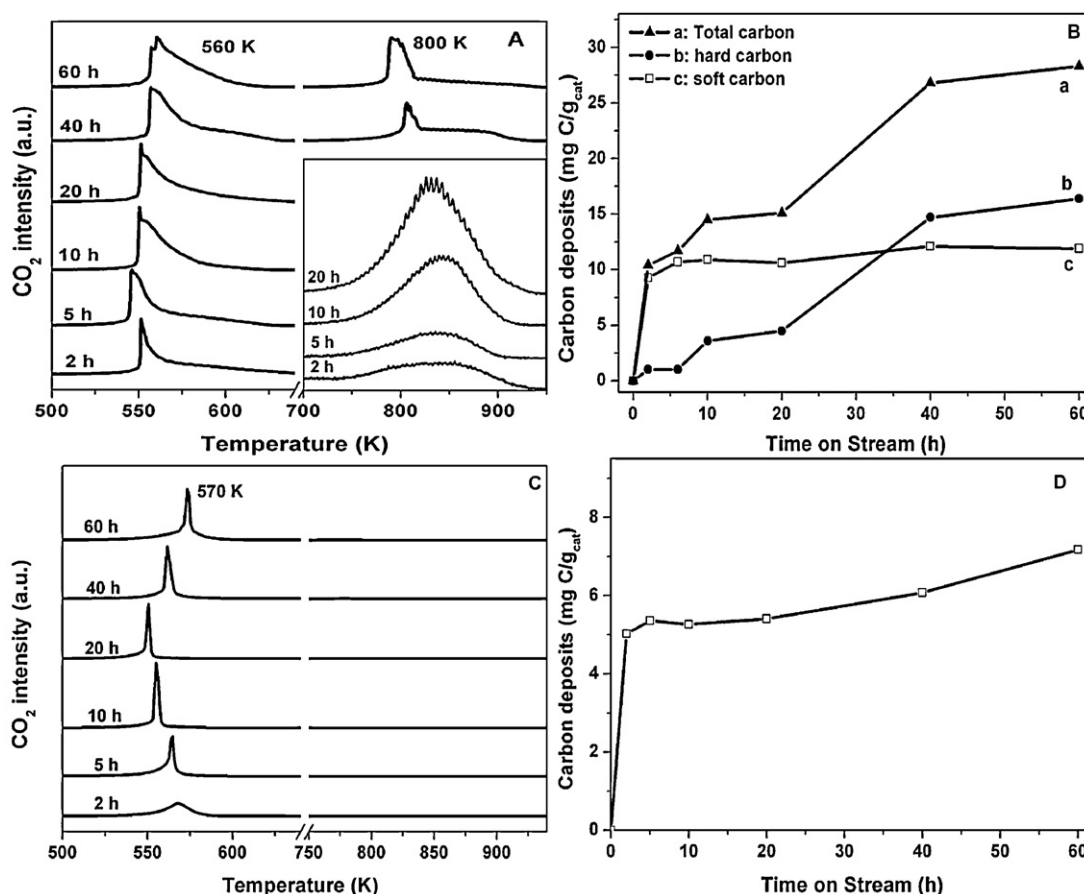


Fig. 10. TPO files (A: 773 K, C: 923 K) and the carbon deposits (B: 773 K, D: 923 K) of the used Ir/CeO₂ catalysts at different time on stream. In Fig. 10A, a zoom of the high temperature range shows the occurrence of HT carbon deposits even after 2 h on stream.

restructuring, as observed by TEM, most likely as a consequence of the steam present under the reacting conditions,

- iii) The Ir particle sintering is significant but to a moderate extent,
- iv) A significant accumulation of carbon deposits, progressively encapsulating the ceria and Ir particles, is observed.

At higher temperature (923 K), the changes in the structure/texture of the catalyst were more significant, as reported in Table 1: the ceria mean grain size increased slightly from 8 to 9 nm, while the sintering of the Ir particles was a little more pronounced (dispersion decrease from 17 down to 9%). The BET surface area again strongly decreased during the first 2 h on stream (from 77 to 57 m² g⁻¹), and decreased regularly to 47 m² g⁻¹ after 60 h on stream, i.e. a little more than at 773 K, as expected from the higher reaction temperature favouring the smoothing and sintering effects. From TEM images (not shown), the major difference compared to the long term run performed at 773 K was the absence of encapsulating carbon, since only traces of carbon could be observed on the sample used at 923 K.

In order to get more information on the carbon deposits, which derive directly from the catalytic performances, a TPO analysis was performed at various temperatures and times on stream.

3.2.4. Analysis of carbon deposits by TPO

Fig. 10 shows the TPO profiles of the used Ir/CeO₂ catalysts at 773 and 923 K and the corresponding amounts of CO₂ produced upon each TPO analysis.

After the ageing test at 773 K (Fig. 10A and B), two domains of CO₂ release, corresponding to different types of carbon deposits, were clearly identified:

- i) The carbon deposits oxidized under TPO conditions at low temperature (named soft or LT carbon, around 560 K) were formed within the first 2 h on stream and then remained practically stable over the whole testing period (Fig. 10B, curve c). From the shape of the LT CO₂ peak (one sharp maximum and a larger shoulder, see Fig. 10A), one could identify at least two types of carbonaceous adspecies with only a slight difference in reactivity. However, due to the lack of more precise data, no deconvolution was attempted.
- ii) The carbon deposits oxidized at higher temperature (named hard or HT carbon, around 800 K) were accumulating progressively with time on stream (Fig. 10B, curve b). Several types of carbon deposits could be proposed but they were not quantified separately.

After the ageing test at 923 K, only a low temperature CO₂ peak was detected by TPO (Fig. 10C and D). It formed very rapidly after the first hours on stream, and increased only slightly with time on stream. Note in addition that this peak was narrower (without shoulder) than the LT peak detected after the ageing test at 773 K and slightly shifted to higher temperature.

The amounts of carbon corresponding to these different adspecies are reported in Table 1 at 773 K and 923 K. Let us discuss now the nature and role of these carbon deposits on the ageing

phenomena, in connection with the changes in morphology and structure reported before.

3.2.5. Origin of the ageing phenomena

The striking coincidence between the initial fast deactivation (Fig. 6), the loss of surface area and the formation of a quasi stable amount of carbon deposits which are highly reactive with oxygen under TPO conditions (soft LT carbon) leads us to propose that this initial period corresponds to a smoothing/restructuring of the surface after ceria re-oxidation by water and its coverage by a layer of reacting carbonaceous adspecies. The latter accumulate rapidly when the initially reduced ceria is oxidized by both the reacting water ($\text{Ce}_2\text{O}_3 + \text{H}_2\text{O} \rightarrow 2\text{CeO}_2 + \text{H}_2$) [32] and possibly the reacting ethanol ($\text{Ce}_2\text{O}_3 + \text{CH}_3\text{CH}_2\text{OH} \rightarrow 2\text{CeO}_2 + \text{CH}_2\text{CH}_2 + \text{H}_2$). The latter reaction would explain the observation of initial traces of ethylene. During this period of time, different reacting intermediates (ethoxy, acetates, carbonates, carbonyls) build up on the surface as shown elsewhere by operando spectroscopy [14,33–35]. Indeed the exact nature of these intermediates strongly depends on various parameters, such as the nature of the catalyst and the operating conditions. Thus, Araque et al. [35] have concluded that essentially carbonates were accumulating on a CeZrCoRh mixed oxide under ethanol SR conditions, leading to the blocking of active sites. For the present case, the formation of carbonates over the same Ir/CeO₂ was clearly identified by DRIFT in our ref [14] but together with acetate adspecies. Therefore, we consider that both acetates and carbonates are reacting intermediates of the ethanol steam reforming (acetates decompose into carbonate and CH_x at metal/support interface) and we have lumped them into the category of “soft” (LT) carbonaceous overlayer built rapidly after the catalyst is contacted to the reacting feed.

To ascertain this assignment, we made a rough calculation of the amount of soft LT carbon deposited per surface oxygen atom of ceria (O_s), from the TPO measured specific carbon deposition and the density of surface oxygen. At 773 K and after 2 h on stream, about 10 mg C g_{cat}^{−1} accumulated over the surface containing about 21 μmol O_s m^{−2}. Considering the final BET surface area of the catalyst (56 m² g^{−1}), the C/O_s ratio was calculated to be ca. 0.7. If one considers that most of the ceria adspecies at such low reaction temperature are C₂ (essentially acetate type) with some C₁ (carbonate type) adspecies, this ratio corresponds to a surface occupancy by the reacting intermediates (including “spectators”) of ca. 1/3. This surface coverage is quite plausible if one assumes a similar coverage by hydroxyl groups as can be foreseen from elementary reaction stoichiometry, e.g. the oxidation of ethoxy species into acetate ($\text{CH}_3\text{CH}_2\text{O}_s + \text{O}_s \rightarrow \text{CH}_3\text{CHO}_s + \text{OH}_s$). It could be added that the shape of the LT TPO peak with a small and sharp peak followed by a large shoulder (Fig. 10 A) could arise from the difference between (i) the adspecies on or in close vicinity of the metal particles where the oxygen dissociates and therefore easily oxidized and (ii) the ones located far away from the metal particles, which requires oxygen spillover along the ceria surface, and therefore slightly higher temperature for being oxidized.

A slightly lower ratio (C/O_s = 0.4) is found when the reaction is performed at 923 K (BET surface area = 47 m² g^{−1}). This indicates a lower surface coverage by the reacting adspecies, which is quite expected at higher temperature. In addition, the higher temperature also changed the nature of the reacting intermediates (possibly more CH_x than C₂) which might explain the already mentioned change in the LT TPO peak shape (Fig. 10 C). The surface metallic sites were not considered here, being in too low concentration as compared to the surface ceria sites (ca. 1%), and therefore only weakly affecting the above reasoning.

To summarize, the initial catalyst start-up period corresponds to both a ceria surface restructuring (loss of microporosity) while it is re-oxidized and the build-up of a reacting adspecies layer (C₂–C₁

adpecies and hydroxyl groups). The latter does not contribute to the long term ageing phenomena.

If one considers now the HT carbon deposits observed essentially at low reaction temperature (773 K), they obviously correspond to the carbon layers progressively encapsulating the catalyst particles (both Ir and ceria), revealed by TEM on Fig. 9. They most likely originate from the polymerization of acetaldehyde and/or ethylene intermediates into amorphous carbon layers, formed in measurable amounts at low testing temperature, as seen previously. Thus, Platon et al. [21] found that co-feeding of ethylene doubled the deactivation rate for ethanol steam reforming over a Rh/Ce–Zr catalyst, which is close to our system. From the TEM and TPO analyses, these amorphous carbon layers are no longer formed at higher reaction temperature, likely due to the fact that the reacting C₂ intermediates are much more easily cracked into syngas at higher temperatures. Therefore, since these “hard” carbon deposits do not accumulate at high temperature, though the catalyst deactivates even faster, as shown on Fig. 7B, these carbon deposits cannot be considered as the main factor responsible for the long-term ageing processes. Note, however, that this statement refers to the present operating conditions, at rather high space velocity and low conversion, therefore not favouring the hard carbon deposition. It might be foreseen that much more severe conditions favouring the accumulation of this type of encapsulating carbon would also lead to long term deactivation. It can be added that for the case of non noble based catalysts (like the cobalt based materials reported in [36,37]), the favoured production of filamentous carbon likely via carbide intermediates might explain serious deactivation at mild temperature, where these filaments are deemed to break the strong metal–support interaction required for allowing the bifunctional process of ethanol SR.

Let us consider now the structural changes in more details. If one accounts for the changes in BET surface area (between 2 and 60 h on stream), it comes that the intrinsic rates (in μmol m^{−2} s^{−1}) reported in Table 1 are about two times larger after 2 h than after 60 h on stream (0.39 vs. 0.18 at 773 K and 3.04 vs. 1.65 at 923 K). Therefore, the small changes in the BET surface area (essentially due to ceria restructuring from spherical crystallites to polygonal cubes) cannot explain the changes in the intrinsic activity. If one considers also the changes in the Ir dispersion due to the metal particle sintering (just by dividing the intrinsic rates by the Ir dispersion), we obtain very close values after 2 and 60 h on stream (1.9 vs. 1.7 at 773 K and 18.2 vs. 17.4 at 923 K) as can be seen in Table 1. Therefore, these simple calculations demonstrate that the long term deactivation observed at any reaction temperature is essentially due to combined changes in both the ceria surface area and the Ir dispersion. This important result is in line with our previous study on the oxidative steam reforming, stating that the interface between the ceria surface and the Ir particles, which depends both on the BET area and the Ir dispersion, essentially monitors the bifunctional mechanism of this reforming reaction over this type of catalysts [15].

Finally, since “pseudo intrinsic” conversion rates (related to the active sites at metal/ceria interface) were obtained after correction of all the deactivating factors, the corresponding intrinsic activation energy has been evaluated from the rate values at 773 and 923 K. It leads to a value of 91 kJ/mol. This value compares rather well with the apparent activation energy values reported in the literature [38] (from 80 to 400 kJ/mol).

4. Conclusions

This study of the ageing of Ir/CeO₂ catalysts under ethanol steam reforming conditions has demonstrated that the changes in catalytic activity and selectivity are due to various factors, depending on the time on stream and the operating conditions. A fast but

moderate deactivation is observed during the initial period on stream (about 2 h) due to a loss of ceria surface (smoothing by loss of microporosity and/or roughness in the presence of steam), coinciding with an active phase build-up, leading to a quasi steady monolayer of C_2-C_1 and OH reacting adspecies over the catalyst surface. Upon longer testing periods (from 2 to 60 h), a slow and continuous sintering of the Ir particles and the ceria crystallites (monitored essentially by the reaction temperature and the presence of steam) leads to an irreversible deactivation essentially due to the degradation of the metal/ceria interface, which controls the cracking of the C_2 adspecies on the ceria surface into CH_x precursors and syngas. At 773 K an encapsulating layer of amorphous carbon is building up from graphite precursors like acetaldehyde and possibly ethylene. This encapsulating carbon layer was not found to be detrimental to the catalytic activity, at least up to 60 h testing and under the present operating conditions. Deactivation effects like mass transfer limitation might be expected for longer times on stream corresponding to industrial applications.

From this ageing analysis, it might be inferred that any marked improvement in catalyst stability would require the stabilization of both the ceria surface area (like doping the ceria with lanthanide ions as shown in [39,40]) and the metal dispersion (by reinforcing the metal-support interaction as shown in [41,42]). In contrast, the rather stable graphite like layer formed at 773 K might be suppressed by catalyst reoxidation from time to time to avoid potential diffusion limitations.

Acknowledgements

Financial support from the National Natural Science Foundation of China (grant no. 20773119) is gratefully acknowledged. The French Embassy in Beijing is kindly acknowledged for the joint PhD student fellowship of Fagen Wang.

References

- [1] T.A. Milne, C.C. Elam, R.J. Evans, Hydrogen from biomass: state of the art and the challenges, IEA/H2/TR-02/001, 2002.
- [2] A. Haryanto, S. Fernando, N. Murali, S. Adhikari, *Energy and Fuels* 19 (2005) 2098–2106.
- [3] P.D. Vaidya, A.E. Rodrigues, *Chemical Engineering Journal* 117 (2006) 39–49.
- [4] M. Ni, D.Y.C. Leung, M.K.H. Leung, *International Journal of Hydrogen Energy* 32 (2007) 3238–3247.
- [5] S.M. de Lima, A.M. Silva, I.O. de Cruz, G. Jacobs, B.H. Davis, L.V. Mattos, F.B. Noronha, *Catalysis Today* 138 (2008) 162–168.
- [6] F. Aupretre, C. Descorme, D. Duprez, *Catalysis Communications* 3 (2002) 263–267.
- [7] T. Yamazaki, N. Kikuchi, M. Katoh, T. Hirose, H. Saito, T. Yoshikawa, M. Wada, *Applied Catalysis B: Environmental* 99 (2010) 81–88.
- [8] A.N. Fatsikostas, X.E. Verykios, *Journal of Catalysis* 225 (2004) 439–452.
- [9] R.C. Cerritos, R.F. Ramirez, A.F.A. Alvarado, J.M.M. Rosales, T.V. Garcia, R.G. Esquivel, *Industrial and Engineering Chemistry Research* 50 (2011) 2576–2584.
- [10] H. Song, U.S. Ozkan, *Journal of Catalysis* 261 (2009) 66–74.
- [11] S. Cavallaro, *Energy and Fuels* 14 (2000) 1195–1199.
- [12] G.A. Deluga, J.R. Salge, L.D. Schmidt, X.E. Verykios, *Science* 303 (2004) 993–997.
- [13] C. Digne, H. Idriss, A. Kiennemann, *Catalysis Communications* 3 (2002) 656–663.
- [14] W. Cai, F. Wang, E. Zhan, A.C. Van Veen, C. Mirodatos, W. Shen, *Journal of Catalysis* 257 (2008) 96–107.
- [15] W. Cai, F. Wang, C. Daniel, A.C. Van Veen, Y. Schuurman, C. Mirodatos, W. Shen, *Journal of Catalysis* 286 (2012) 137–152.
- [16] H. Chen, H. Yu, F. Peng, H. Wang, J. Yang, M. Pan, *Journal of Catalysis* 269 (2010) 281–290.
- [17] S.M. Lima, A.M. Silva, L.O.O. Costa, U.M. Graham, G. Jacobs, B.H. Davis, L.V. Mattos, F.B. Noronha, *Journal of Catalysis* 268 (2009) 268–281.
- [18] C.H. Bartholomew, *Applied Catalysis A: General* 212 (2001) 17–60.
- [19] A.M. da Silva, L.O.O. da Costa, K.R. Souza, L.V. Mattos, F.B. Noronha, *Catalysis Communications* 11 (2010) 736–740.
- [20] H.S. Roh, A. Platon, Y. Wang, D. Wang, *Catalysis Letters* 110 (2006) 1–6.
- [21] A. Platon, H.S. Roh, D.L. King, Y. Wang, *Topics in Catalysis* 46 (2007) 374–379.
- [22] S. Freni, S. Cavallaro, N. Mondello, L. Spadaro, F. Frusteri, *Catalysis Communications* 4 (2003) 259–268.
- [23] L.P.R. Profeti, E.A. Ticianelli, E.M. Assaf, *Journal of Power Sources* 175 (2008) 482–489.
- [24] J.M. Guil, N. Homs, J. Llorca, P.R. de la Piscina, *Journal of Physical Chemistry B* 109 (2005) 10813–10819.
- [25] T. Montini, L. de Rogatis, V. Gombac, P. Fornasiero, M. Graziani, *Applied Catalysis B: Environmental* 71 (2007) 125–134.
- [26] B.D. Cullity, *Elements of X-Ray Diffraction*, Addison-Wesley, Menlo Park, CA, 1978.
- [27] P. Fornasiero, J. Kaspar, M. Graziani, *Journal of Catalysis* 167 (1997) 576–580.
- [28] W.C. Conner, J.L. Falconer, *Chemical Reviews* 95 (1995) 759–788.
- [29] G. Rabenstein, V. Hacker, *Journal of Power Sources* 185 (2008) 1293–1304.
- [30] W.-I. Hsiao, Y.-S. Lin, Y.-C. Chen, C.-S. Lee, *Chemical Physics Letters* 441 (2007) 294–299.
- [31] M. Pijolat, M. Prin, M. Soustelle, P. Nortier, *Journal de Chimie Physique* 91 (1994) 51–62.
- [32] F. Sadi, D. Duprez, F. Gerard, A. Miloudi, *Journal of Catalysis* 213 (2003) 226–234.
- [33] A. Yee, S.J. Morrison, H. Idriss, *Journal of Catalysis* 186 (1999) 279–295.
- [34] J. Rasko, A. Hancz, A. Erdohelyi, *Applied Catalysis A: General* 269 (2004) 13–25.
- [35] M. Araque, J.C. Vargas, Y. Zimmermann, A.C. Roger, *International Journal of Hydrogen Energy* 36 (2011) 1491–1502.
- [36] H. Wang, Y. Liu, L.Y. Wang, N. Qin, *Chemical Engineering Journal* 145 (2008) 25–31.
- [37] A.E. Galetti, M.F. Gomez, L.A. Arrua, A.J. Marchi, M.C. Abello, *Catalysis Communications* 9 (2008) 1201–1208.
- [38] C. Graschinsky, M. Laborde, N. Amadeo, A. Le Valant, N. Bion, F. Epron, D. Duprez, *Industrial and Engineering Chemistry Research* 49 (2010) 12383–12389.
- [39] B.M. Reddy, L. Katta, G. Thrimurthulu, *Chemistry of Materials* 22 (2010) 467–475.
- [40] F. Wang, W. Cai, H. Provendier, Y. Schuurman, C. Descorme, C. Mirodatos, W. Shen, *International Journal of Hydrogen Energy* 36 (2011) 13566–13574.
- [41] G. Zhou, L. Barrio, S. Agnoli, S.D. Senanayake, J. Evans, A. Kubacka, M. Estrella, J.C. Hanson, A.M. Arias, M.F. Garcia, J.A. Rodriguez, *Angewandte Chemie International Edition* 49 (2010) 9680–9684.
- [42] S. Bernal, J.J. Calvino, M.A. Cauqui, J.M. Gatica, C. Larese, J.A.P. Omil, J.M. Pintado, *Catalysis Today* 50 (1999) 175–206.